**Showcasing research from Associate Professor Dr Mintu Porel's laboratory, Department of Chemistry, Indian Institute of Technology Palakkad, Kerala, India.**

Fluorescent hyperbranched polymers with a tunable backbone: design, synthesis and application in coloring and anti-counterfeit

The work presents dansyl-tagged, functionally tunable fluorescent hyperbranched polymers (HBPs) containing 1,2,3-triazole linkages that serve as efficient dye-capturing systems by trapping and retaining water-soluble dyes from aqueous environments. Their cavity-rich architecture facilitates strong host–guest interactions, effectively preventing dye leaching and ensuring excellent long-term color stability. The encapsulation efficiency was precisely modulated by altering the functional substituents on the polymer backbone. This intrinsic ability highlights their potential for purifying dye-contaminated water and generating durable, water-resistant colored materials, while their fluorescence enables promising use in anti-counterfeit and multifunctional material applications.

As featured in:

ROYAL SOCIETY OF CHEMISTRY

rsc.li/materials-advances

PAPER

Check for updates
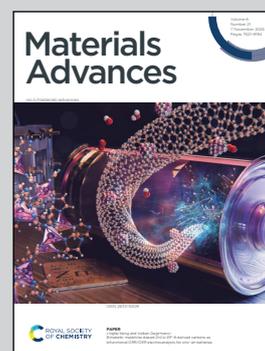
Fluorescent hyperbranched polymers with a tunable backbone: design, synthesis and application in coloring and anti-counterfeit

Geethanjali Anand[a] and Mintu Porel (ID) ⋆[ab]

Hyperbranched polymers (HBPs) are intricately branched macromolecules with a three-dimensional, tree-like architecture rich in internal cavities, making them ideal for encapsulating guest molecules and facilitating host–guest interactions. In this study, functionally tunable HBPs with 1,2,3-triazole linkages were synthesized *via* a copper-catalyzed azide–alkyne cycloaddition (CuAAC) reaction between custom-designed azide and alkyne monomers. Strategic modification of the monomeric units enabled the synthesis of two distinct HBPs, which were thoroughly characterized using FTIR, NMR, TGA-DTA, SEM-EDAX, XRD, DSC, cyclic voltammetry, and steady-state and time-resolved spectroscopy. Tailoring the functional groups modulated key properties such as hydrophobicity, thermal stability, and electrochemical and photophysical behavior. Notably, dansyl-functionalized HBPs exhibited robust fluorescence in both solid and solution phases, which was harnessed for anti-counterfeit applications, offering a durable and secure luminescent marker. Furthermore, incorporating aromatic units enhanced the electrical conductivity of the HBPs. Their host–guest capabilities were demonstrated through efficient encapsulation of four water-soluble dyes—Congo red, Rose Bengal, methyl orange, and fluorescein sodium—with no observable release, indicating strong retention. This dye encapsulation approach was applied to fabricate water-resistant, colored plastic membranes, addressing dye leaching—a common limitation in conventional systems. By minimizing dye release into water bodies, these HBPs serve as environmentally sustainable coloring agents, offering a compelling route toward pollution reduction and enhanced material performance.

1. Introduction

Hyperbranched polymers (HBPs) belong to the category of dendritic polymers and are characterized by an exceptionally dense branching structure, offering the capability of branching within each repeating unit.[1] The distinct characteristics of HBPs are rooted in their intricately branched three-dimensional configuration, internal voids, and numerous reactive end groups distributed extensively on the surface. Owing to these exceptional features, HBPs exhibit unique physicochemical properties, such as low intrinsic viscosity, high solubility, and multifunctionality, which make them attractive materials for a wide range of applications.[2,3]

HBPs stand apart from their linear counterparts and dendrimers in terms of synthetic accessibility and functional complexity. While dendrimers involve laborious multi-step syntheses with rigorous purification at each stage, HBPs can be prepared through simpler one-pot procedures, making them attractive for large-scale production.[4] Despite this advantage, many existing synthetic approaches provide limited control over polymer architecture, resulting in random branching and uneven functional distribution. These challenges have driven the need for methods that preserve the ease and scalability of HBP synthesis while enabling greater precision in backbone design and functional tunability factors that are crucial for tailoring material properties for specific applications.

HBPs are well-recognized for their host–guest encapsulation abilities, stemming from their internal cavities and abundant surface groups. These properties have been explored for the encapsulation of dyes,[5] fragrances,[6] drugs,[7] catalysts,[8] and polycyclic aromatic hydrocarbons.[9] However, many of these studies involve non-fluorescent HBPs or focus on post-encapsulation modifications, rather than intrinsically functional HBPs that integrate host–guest chemistry with photophysical properties. Furthermore, systematic correlations between the polymer structure (*e.g.*, nature of branching units) and encapsulation efficiency or guest selectivity remain underexplored.

[a] *Department of Chemistry, Indian Institute of Technology Palakkad, Kerala-678623, India. E-mail: mintu@iitpkd.ac.in*

[b] *Environmental Sciences and Sustainable Engineering Centre, Indian Institute of Technology Palakkad, Kerala-678623, India*

To address these limitations, we developed a modular and scalable strategy to synthesize a novel class of triazole-based HBPs *via* copper-catalyzed azide–alkyne cycloaddition (CuAAC) click chemistry. This approach offers control over both backbone architecture and side-chain functionalization, enabling structural tuning with minimal synthetic complexity. Functional tunability is crucial for tailoring HBPs toward targeted applications, as small structural changes can modulate solubility, cavity polarity, aromaticity, and optical behavior.[10,11] For instance, replacing a flexible propyl linker with a rigid, aromatic xylylene unit significantly enhanced the polymer's conjugation and internal rigidity factors known to affect the overall properties, as well as host–guest interactions.

Fluorescence was imparted by incorporating dansyl moieties into the polymer side chains, producing HBPs with stable photoluminescence. While fluorescent dendrimers have been studied for sensing and imaging,[12,13] analogous fluorescent HBPs with controlled emission and cavity structure remain rare, especially those synthesized *via* scalable routes. The materials reported here thus offer a dual-function system combining host–guest capability with fluorescent tracking, suitable for advanced applications such as anti-counterfeiting.

Encapsulation studies using water-soluble dyes further validated the host capability of the synthesized HBPs. The strong interaction between the guest dye and the polymer cavities led to the formation of dye-loaded fluorescent systems, which may serve as novel co-colorants in plastic materials.[14–16] Conventional colorants often migrate out of polymer matrices due to weak intermolecular interactions, causing fading, contamination, and environmental hazards.[17,18] Although some approaches have explored dendritic additives to suppress migration,[19,20] the use of hyperbranched fluorescent systems for stable dye encapsulation and migration resistance remains largely unexplored.

In this context, the current work fills an important gap by offering a structurally tunable, photoluminescent, and host-capable HBP system, synthesized *via* a robust and industry-compatible method. These materials provide a foundation for next-generation multifunctional polymers applicable in anti-counterfeiting, smart packaging, and sustainable plastic coloration.

2. Experimental methods

2.1. Materials

The chemicals utilized in this study were sourced from reputable suppliers, including Sigma Aldrich, Alfa Aesar, Spectrochem, Merck, and TCI. Analytical grade solvents like chloroform, methanol, dimethyl sulphoxide, dichloromethane, acetone, and acetonitrile were employed without further purification.

2.2. Synthesis

2.2.1. Synthesis of tetrayne precursors. For the synthesis of tetrayne precursor **3a** (Scheme 1), propane-1,3-diamine was added to 1 mL DMF solvent. To this, sodium hydride was added, followed by the slow addition of propargyl bromide. The reaction mixture was stirred at room temperature for 1 hour. The product formed was subjected to washing with a mixture of ethyl acetate and water. The product in the ethyl acetate layer was passed through anhydrous sodium sulphate, followed by evaporation of solvent under reduced pressure to obtain the product. The synthesis of tetrayne precursor **3b** (Scheme 1) was initiated with the selection of *m*-xylylene diamine as the starting amine. Following this, the synthesis followed identical steps to those outlined for the tetrayne precursor **3a** (Scheme 1).

2.2.2. Synthesis of diazide precursors. Diethanolamine was dissolved in chloroform, followed by the slow addition of thionyl chloride to initiate the chlorination reaction. Dimethylformamide (DMF) was introduced to serve as a catalyst. The resulting mixture was then refluxed at 60 °C for 30 minutes, yielding dichlorodiethylamine as a solid mass (Scheme S3). Subsequently, this dichlorodiethylamine was subjected to a reaction with sodium azide in water at 60 °C for 12 hours, leading to the formation of diazide precursor **D1** (Scheme S4). Diazide precursor **D1** was further employed in the synthesis of diazide precursor **D2** (Scheme S5). In this step, diazide precursor **D1** (Scheme S4) underwent reaction with dansyl chloride in the presence of *N*,*N*-diisopropylethylamine as the base. The reaction mixture was refluxed at 70 °C for 3 hours in chloroform, resulting in the formation of fluorescent diazide precursor **D2** (Scheme S5).

2.2.3. Synthesis of hyperbranched polymers (HBPs). The synthetic strategy for both the HBPs involved the cycloaddition reaction between the diazide and tetrayne *via* click reaction. The difference in the synthetic method for each HBP comes from the difference in the combination of the diazide and tetrayne precursor. For **HBP1**, diazide precursor **D2** and tetrayne precursor **3a** (Scheme S6) were used, whereas for **HBP2**, diazide precursor **D2** and tetrayne precursor **3b** (Scheme S7) were taken. To the diazide and tetrayne taken in a solvent system comprising water and methanol in a 1:1 proportion, $CuSO_4 \cdot 5H_2O$ was added as the catalyst and sodium-L-ascorbate as the reducing agent. The reaction was kept at 60 °C for 24 hours. The formation of HBP was indicated by the appearance of solid particles insoluble in the reaction mixture. This was filtered, washed with distilled water multiple times to remove any water-soluble impurities, followed by washing with acetone. The product was then air-dried at room temperature for 24 hours, followed by an additional 48 hours of drying in an oven set at 60 °C.

2.3. General procedure for the encapsulation of dyes in HBPs

Four water-soluble dyes, Congo red (CR), methyl orange (MO), fluorescein sodium (FS), and Rose Bengal (RB), were employed in encapsulation studies involving two distinct hyperbranched polymers designated as **HBP1** and **HBP2** (Schemes S6 and S7). Solutions of the four dyes were prepared at a concentration of 100 ppm in water, while a stock solution of HBPs at 1 mg mL^{-1} was prepared in chloroform. Subsequently, 500 µL volumes of each dye solution and each HBP were transferred to individual vials. The resulting two layers, aqueous and chloroform, were
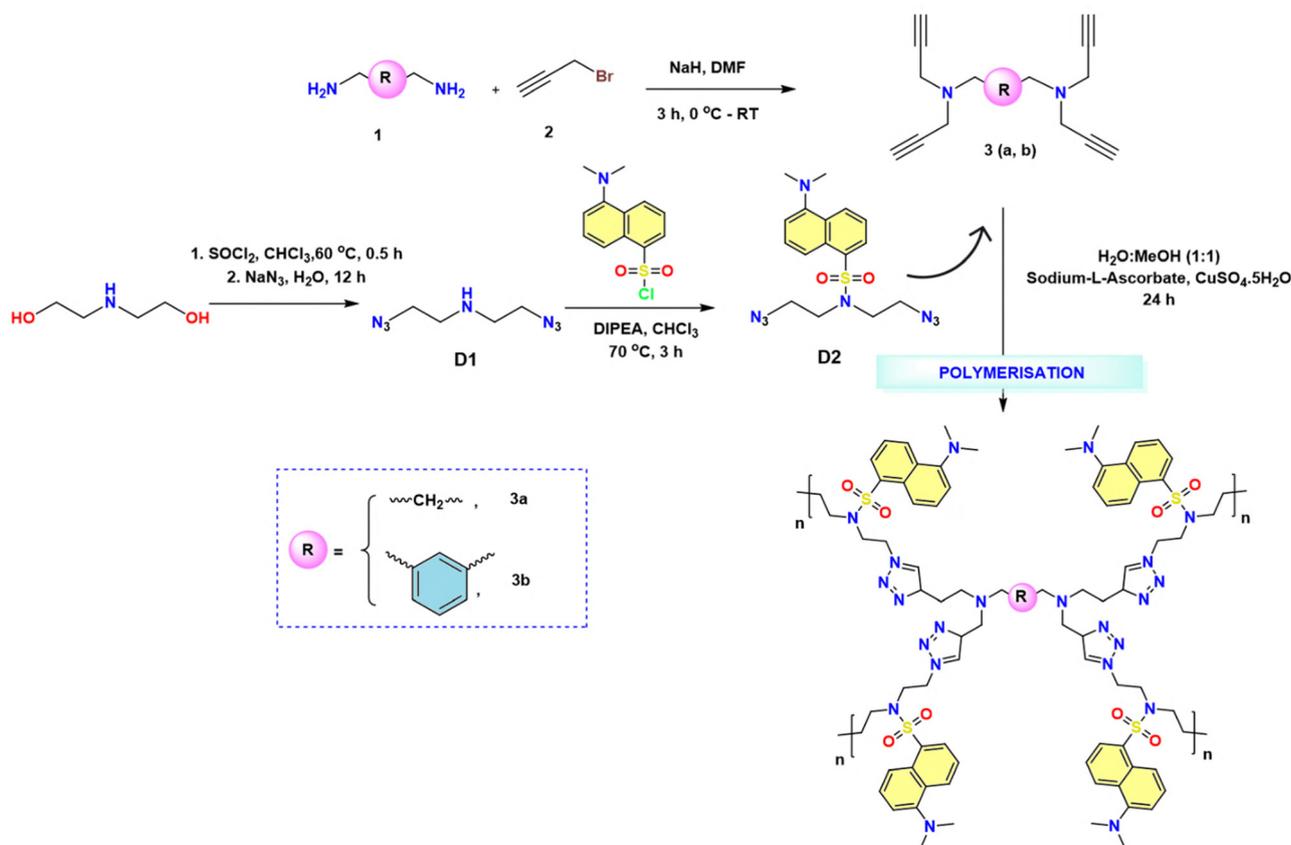
Scheme 1 General scheme for the synthesis of the triazole-based hyperbranched polymer.

vigorously shaken to facilitate the extraction process. Concurrently, a control experiment was conducted wherein 500 μL of each dye solution was used as the aqueous layer, and instead of the HBP solutions, pure chloroform solvent was taken as the organic layer. The extraction procedures were then conducted in the same manner as described previously.

2.4. Release studies of the encapsulated guest (dyes)

The dye-encapsulating polymer particles, obtained by evaporating the HBPs system in chloroform, were placed in a vial with 50 mL of distilled water (pH 7). The suspension was agitated in a bath shaker at room temperature to facilitate release. A sample was periodically taken, and the concentration of dye was determined *via* UV-vis spectroscopy to monitor release kinetics under neutral conditions.

2.5. Procedure for coloring applications of polymer

Here, 1 g of polystyrene (PS) was dissolved in 10 mL of chloroform and blended with 2.0 mL of a chloroform solution containing polymer–dye complexes, yielding vibrant, transparent polymer solutions. These solutions were carefully poured into a culture dish, allowing for the gradual evaporation of chloroform at room temperature over 24 hours. Subsequently, the samples were subjected to a meticulous drying process in an oven set at 60 °C for 72 hours, resulting in the formation of sturdy, colored free-standing membranes upon peeling.

To ensure a comprehensive comparison, control samples were prepared by directly mixing polymer solutions with dye powders, following the identical treatment process described above. The resulting dye-colored polymer membranes were uniformly cut into circular shapes of similar dimensions. These strips were immersed in distilled water at room temperature, which served as a method to evaluate the color stability of the membranes.

3. Results and discussion

3.1. Design and synthesis of hyperbranched polymers (HBPs)

A novel method for synthesizing triazole-based hyperbranched polymers (HBPs) with tunable properties is described herein. This approach necessitates the precise incorporation of custom-designed starting materials at predetermined positions using the alkyne–azide click reaction. Tunable characteristics in both the backbone and side chains were attained through the synthesis of two different alkynes, each possessing diverse functionalities. Scheme 1 illustrates the general synthetic strategy for the HBPs. Firstly, the diamine system with the desired functional group R (Scheme 1) was reacted with propargyl bromide at 0 °C in 1 mL of DMF as the solvent. Subsequently, sodium hydride was introduced, and the reaction was maintained for 3 hours to obtain product **3(a, b)**, which is the tunable tetrayne precursor molecule (Scheme 1). By modifying

the R moiety of the diamine precursor (Scheme 1), two distinct tetrayne precursors, **3a** (Scheme S1) and **3b** (Scheme S2), were synthesized. **3a** contains a propyl functionality in the backbone, whereas **3b** incorporates a xylylene functionality. The synthesis of diazide precursor **D1** proceeded in two steps. Firstly, diethanolamine was reacted with thionyl chloride at 60 °C to obtain the chlorinated product (Scheme S3). Subsequently, the resulting chlorinated product was treated with sodium azide at 70 °C in the second step to yield diazide precursor **D1** (Scheme S4). Further, diazide precursor **D1** was subjected to reflux conditions along with dansyl chloride at 70 °C to yield the diazide precursor **D2** (Scheme S5). Following the synthesis of the tetrayne and diazide precursors, the tetrayne precursor with tunable functional group R was treated with diazide precursor **D2** under reflux conditions to produce two hyperbranched polymers, named **HBP1** and **HBP2**. Polymer **HBP1** features a propyl unit in its backbone, while **HBP2** contains a xylylene backbone. Notably, transitioning from **HBP1** to **HBP2** reflects an increase in the overall aromatic content of the HBPs due to the greater presence of aromatic structures within their compositions.

3.2. Characterization

The characterization of the synthesized HBPs was conducted using various analytical techniques. Initially, infrared (IR) spectroscopy was employed to monitor the conversion of the starting material azide to the polymer. The disappearance of the azide peak at 2094 cm^{-1} and the appearance of characteristic triazole peaks around 2930 cm^{-1} confirmed the formation of the polymer *via* triazole linkages (Fig. 1a and Fig. S10). This was further confirmed by ^{1}H NMR spectroscopy, which indicated the presence of all protons within the polymer structure (Fig. 1b). The emergence of a new peak at 7.5 ppm

corresponding to the triazole proton peak in the NMR spectrum of **HBP1** and **HBP2** confirmed the successful formation of the polymer *via* alkyne–azide cycloaddition (Fig. 1b). This transformation is indicative of the conversion of the alkyne functionality into the triazole linkage within the polymer structure. Furthermore, the absence of peaks in the aromatic region of the tetrayne precursor **3a** (Scheme S1), owing to the lack of any aromatic protons, contrasts sharply with the presence of distinct peaks between 7.1 and 8.6 ppm in the ^{1}H NMR spectrum of **HBP2** (Fig. 1b). These peaks validate the incorporation of the dansyl moiety from diazide precursor **D2** (Scheme S5) into the polymer framework. Collectively, these observations serve as evidence affirming the formation of the hyperbranched polymers from the diazide and tetrayne precursors. Further, ^{1}H–^{1}H COSY was carried out to understand the correlations (Fig. S11). For **HBP1**, clear cross-peaks were observed in both aromatic and aliphatic regions. In the aromatic region, correlations appeared between h–i, i–m, j–k, and l–j protons, while in the aliphatic region, proton b showed correlation with proton a. For **HBP2**, a correlation was detected between the aromatic protons h and i, in agreement with the expected structural framework. The precursor molecules were also characterized using LC-MS analysis (Fig. S1–S9). Morphological examination of the polymers was carried out using scanning electron microscopy (SEM), revealing distinct morphologies attributed to differences in their chemical compositions (Fig. 2 and Fig. S12). Elemental analysis and elemental mapping of the polymer were performed using energy dispersive X-ray analysis (EDAX), which provided the elemental composition consistent with the expected polymer constitution (Fig. 2 and Fig. S13).

Thermal properties of the polymers were assessed through thermogravimetric analysis-differential thermal analysis (TGA-DTA) (Fig. 3a). TG-DTA analysis indicated that both HBPs
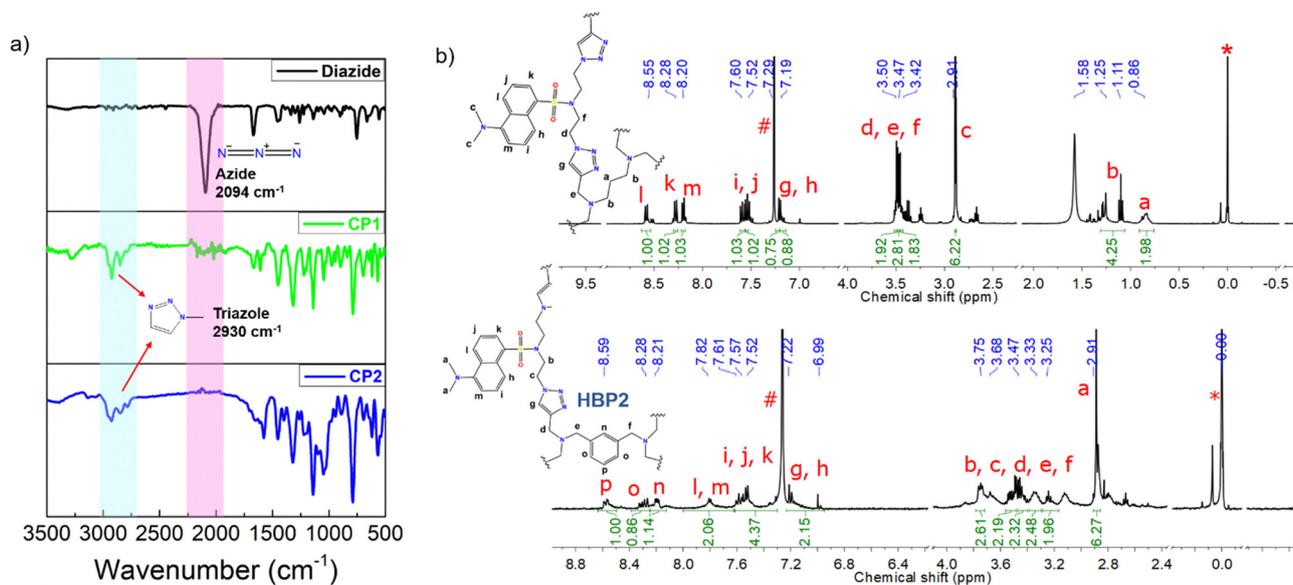

Fig. 1 Characterization of hyperbranched polymer **HBP1**: (a) ATR-FTIR spectra highlighting the emergence of a new triazole peak in **HBP1** (bottom) and the complete disappearance of the azide peak (top), confirming successful cycloaddition. (b) ^{1}H NMR spectra of **HBP1** and **HBP2** polymers in CDCl$_3$ solvent (# and * represent residual proton peaks of CDCl$_3$ and TMS, respectively).
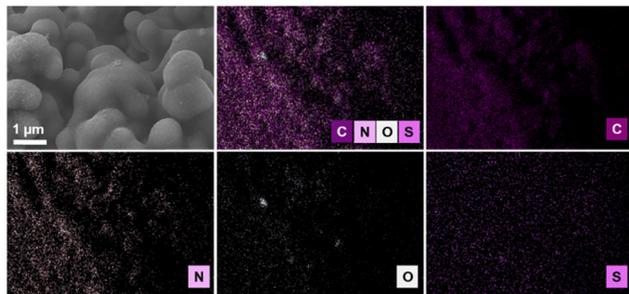
Fig. 2 FESEM image (top-left) showing the surface morphology and elemental mapping images showing the elemental composition of HBP1.

exhibited stability up to the temperature range of 200 °C to 300 °C. Furthermore, a notable correlation emerged between thermal stability and the aromatic content of the polymers. Specifically, as the number of aromatic moieties within the polymer increased from **HBP1** to **HBP2**, the thermal stability was enhanced. Powder X-ray diffraction analysis (XRD) confirmed the amorphous nature of the polymers, possibly due to their hyperbranched structures (Fig. 3b). To ascertain the glass transition temperatures (T_g), differential scanning calorimetry (DSC) analysis was conducted (Fig. 3c). In resonance with the TGA values, a lower T_g value of 12.39 °C was observed for **HBP1**, while a slightly higher value of 17.45 °C was obtained for **HBP2**.

The solubility of the synthesized HBPs was evaluated in water and various organic solvents. Notably, both HBPs displayed complete insolubility in water, while solubility was observed in specific organic solvents. Leveraging the solubility of **HBP1** and **HBP2** in DMSO, conductometric studies were conducted (Fig. 3d). Both polymers demonstrated conductive properties; however, **HBP2** exhibited significantly higher conductance compared to **HBP1** (Fig. 3d). This difference in

conductance is likely linked to the higher aromatic content present in **HBP2** compared to **HBP1**. Aromatic rings provide delocalized π-electrons, facilitating electron movement along the polymer backbone, thereby augmenting electrical conductivity.[21-23] Cyclic voltammetry studies were further performed to assess the electrochemical stability of both HBPs. The results showed that both polymers maintained exceptional stability over five consecutive cycles, as depicted in Fig. S14, highlighting their robustness under repeated redox conditions.

3.3. Photophysical characteristics of HBPs

The incorporation of the dansyl moiety within the polymer backbone conferred fluorescence properties upon the HBPs. This was investigated using fluorescence spectrophotometry and time-correlated single photon counting (TCSPC) analytical techniques. Notably, both polymers demonstrated robust solid-state fluorescence. The photographic image of the solid-state fluorescence of **HBP2** under UV illumination and its corresponding fluorescence spectrum are presented in Fig. 4a and Fig. S15, respectively. The lifetimes of both **HBP1** and **HBP2** calculated from TCSPC analysis are 3.33 ns (Fig. S16b) and 4.91 ns (Fig. 4b), respectively. The quantum yields of **HBP1** and **HBP2** were determined to be 0.24 and 0.15 (Fig. S17), respectively. Additionally, the HBPs displayed positive solvatochromic behavior upon dissolution in a range of solvents, each varying in polarity index (Fig. 4c and d). The dansyl monomer (azide precursor) showed emission maxima at ~465 nm in chloroform (Fig. S18), whereas **HBP1** and **HBP2** exhibited red-shifted maxima near 500 nm, reflecting electronic perturbations from polymerization. In THF/water mixtures (Fig. S19), both polymers displayed progressive red-shifts (**HBP1**: 512 → 559 nm; **HBP2**: 514 → 555 nm) with reduced intensity as the water fraction increased, indicating aggregation-induced quenching (ACQ) due to poor solubility and π–π stacking of dansyl units.
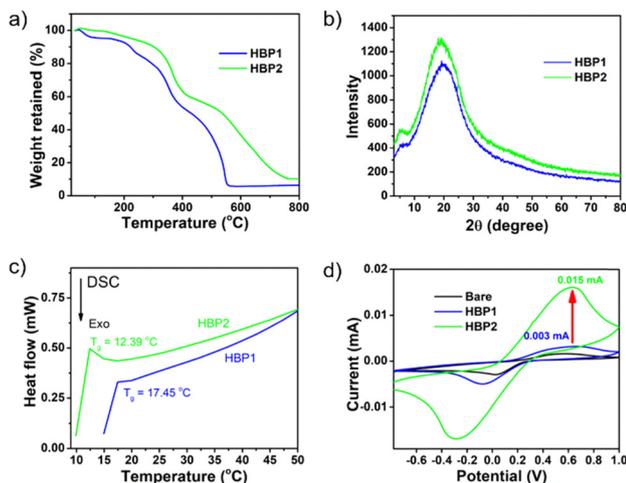

Fig. 3 (a) TG-DTA profiles showing temperature dependence, (b) XRD patterns showing the amorphous nature, and (c) DSC plots comparing glass transition temperatures of **HBP1** and **HBP2**. (d) Cyclic voltammetry plots for bare, **HBP1**, and **HBP2** recorded in aq. 10 mM K$_3$[Fe (CN)$_6$] + 0.1 M KCl at a scan rate of 200 mV s^{-1} vs. saturated calomel electrode, showing the higher conducting nature of **HBP2** over **HBP1**.
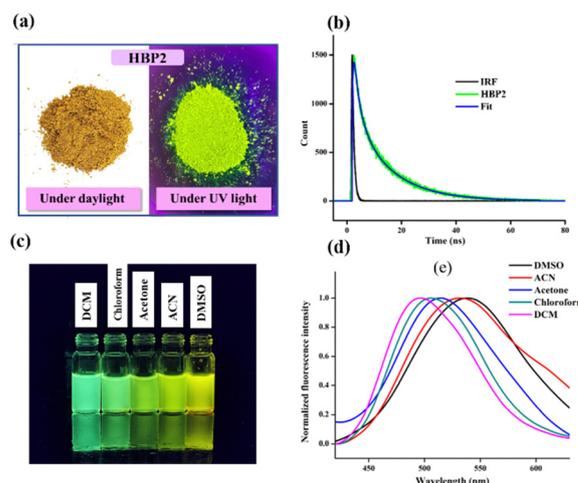

Fig. 4 Photophysical characteristics of **HBP2**: (a) photographs of **HBP2** under daylight and UV light. (b) Time-correlated single-photon counting (TCSPC) analysis. (c) Photograph showing solvatochromism. (d) Fluorescence spectra of solvatochromism on excitation of 20 μg mL^{-1} of **HBP2** solutions in different solvents at λ_{ex} = 330 nm.

3.4. Encapsulation of water-soluble dyes

Due to the cavity-like spaces within the branches of the HBPs, these two polymers were used to investigate the encapsulation of four water-soluble dyes: Congo red, Rose Bengal, methyl orange, and fluorescein sodium. These dyes are highly soluble in water but inherently insoluble in chloroform when taken alone. However, when a chloroform solution containing either **HBP1** or **HBP2** was used for liquid–liquid extraction, the dyes were efficiently transferred from the aqueous phase to the organic phase, as illustrated in Fig. 5. In contrast, no color change was observed in the organic layer in the absence of HBPs, confirming that the transfer was facilitated by the polymers. To determine whether this behavior was due to the dansyl moiety alone or required the full polymer architecture, a control extraction was carried out using free dansyl chloride in chloroform. No dye transfer occurred under these conditions (Fig. S21), indicating that the cooperative effect of the hyperbranched architecture and the dansyl groups is essential for enabling the efficient encapsulation and phase transfer of the dyes.

Further comparative studies of dye encapsulation were conducted between **HBP1** and **HBP2** using four water-soluble dyes. A higher efficiency in dye transfer was observed for **HBP2** compared to **HBP1** for all four dyes. Fig. 5 represents the photographic images showing the extraction of the four water-soluble dyes from the aqueous layer to the chloroform layer containing HBPs, along with their corresponding UV-vis spectra. This can be attributed to the increased π–π interactions possible between **HBP2** and the dyes in comparison to **HBP1**. Since these dyes are essentially organic molecules containing

Table 1 Dye-transfer efficiency of the HBPs with the four water-soluble dyes having a concentration of 100 ppm in water

Dyes (100 ppm)	Dye transfer efficiency (DTE) %	
	HBP1	**HBP2**
Rose Bengal (RB)	99.06	99.45
Congo red (CR)	94	96
Methyl orange (MO)	62	88
Fluorescein sodium (FS)	26.45	30.2

aromatic moieties, **HBP2**, with its repeating units of xylylene moieties along with dansyl and triazole groups, offers greater opportunities for π–π interactions. Conversely, **HBP1**, with propyl units instead of xylylene units, reduces the extent of π–π interactions, which reduces its dye transfer efficacy. Table 1 shows the obtained dye transfer efficiency (DTE) values for **HBP1** and **HBP2** for all four dyes. The values clearly indicate the influence of aromatic units within the polymer on dye encapsulation. Among the dyes, RB exhibited an exceptional DTE of over 99% with both HBPs. CR also showed a high DTE, exceeding 94%. MO achieved a DTE of 88% with **HBP2** and over 60% with **HBP1**. In contrast, FS displayed minimal encapsulation. To probe the photophysical changes associated with dye encapsulation, emission spectra of both polymers were recorded before and after encapsulation of RB and CR (Fig. S20). Encapsulation of RB into **HBP1** and **HBP2** resulted in noticeable quenching of the polymer emission along with the emergence of a new band at $\sim$590 nm, corresponding to RB emission when excited at 330 nm. Importantly, RB alone displayed only weak emission at this wavelength under identical excitation, whereas the encapsulated form showed much stronger emission, suggesting that the local polymer environment enhances RB fluorescence. In contrast, CR encapsulation caused only a minor quenching of polymer fluorescence without any new emission features.

3.5. Release studies of the dyes by HBPs

Release studies were carried out to assess the efficacy of encapsulating dye molecules within the cavities of **HBP1** and **HBP2**. Given the inherent water solubility of the dyes, their release upon exposure to water serves as a pivotal indicator of encapsulation strength. Robust encapsulation should effectively retain the dyes within the polymer cavities, impeding their release into the surrounding aqueous environment. Conversely, weak encapsulation would result in the facile release of the water-soluble dyes into the water medium. Given that CR and RB exhibited higher dye transfer efficiencies (DTE), these two dyes were selected for the release studies. The particulates of both the dye–HBP composites, obtained after evaporating the chloroform layer following extraction, were suspended in water (pH 7), and the resulting solutions were shaken at room temperature, and the release of dyes was monitored at specific time intervals for 100 hours. Fig. S23 illustrates the results of the dye release. The amount of dyes released from the dye–HBP composite was monitored using UV-Vis spectroscopy at a wavelength 498 nm for CR and 548 nm for RB. The results
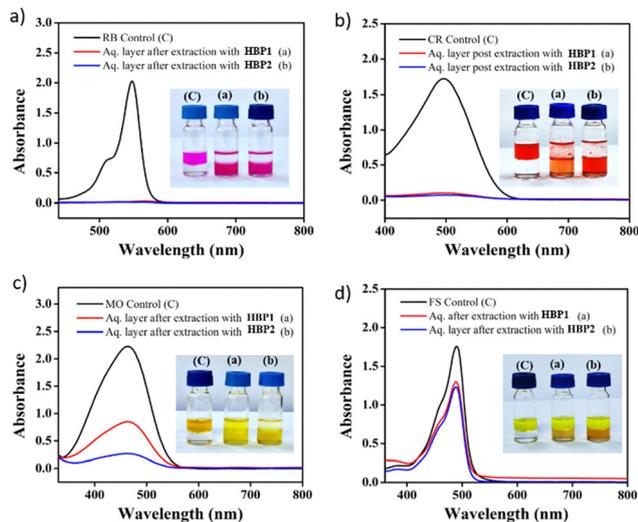

Fig. 5 UV-vis spectra of residual water-soluble dyes: (a) Rose Bengal (λ_{ex} = 548 nm), (b) Congo red (λ_{ex} = 498 nm), (c) methyl orange (λ_{ex} = 464 nm) and (d) fluorescein sodium (λ_{ex} = 490 nm) in aqueous solution post-extraction with chloroform solutions of hyperbranched polymers **HBP1** and **HBP2** along with their corresponding vial pictures, highlighting the effects of functional groups on dye removal (the upper layer in the vial picture is water and the bottom layer is chloroform). Dye solutions taken before extraction were 100 ppm.

clearly indicate that both **HBP1** and **HBP2** effectively retained the dye molecules, with less than 10% being released when exposed to water. Remarkably, the release percentage for Rose Bengal was even lower, at less than 2%, showcasing the strength of encapsulation provided by these HBPs.

3.6. Coloring applications of the dye-encapsulated HBP

Owing to their remarkable capability to retain dyes within their cavity, the HBP–dye composites were specifically chosen for use in coloring plastic membranes. Fig. 6 depicts the resulting colored plastic membranes achieved through the utilization of **HBP2**–dye composites with three water-soluble dyes: CR, MO, and RB. The colored polystyrene (PS) membranes were fabricated by incorporating the HBP–dye composite into a chloroform solution of polystyrene. The solution was then subjected to solvent evaporation, followed by a thorough drying procedure to ensure optimal membrane formation. To ascertain the durability of the colored membranes and their resistance to decolorization upon exposure to aqueous environments, release studies were conducted by taking the **HBP2-RB** membrane as the model. Remarkably, the results clearly demonstrated that the colored membrane did not release dyes into the water phase, even after a period of 4 months. Conversely, control experiments involving the use of dyes alone for coloring the plastic membranes revealed significant dye release upon contact with the aqueous layer (Fig. S24).
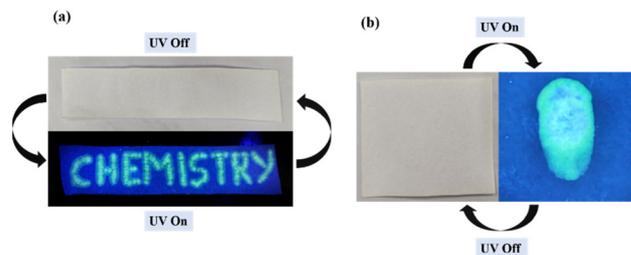
Fig. 7 Photographic images of the application of the DMSO solution of **HBP2** as an anticounterfeiting security material: (a) as letters and (b) as a fingerprint coated on Whatman filter paper using 1 mg mL^{-1} **HBP2**.

3.7. Anticounterfeit application of the dansyl-appended HBPs

Anti-counterfeit applications are important since they safeguard consumers from counterfeit goods by ensuring product authenticity through reliable verification methods. Fluorescent molecules are used in anti-counterfeit measures by embedding them into products or packaging to create unique, verifiable markers that authenticate genuine items and detect counterfeit ones.[24] This fluorescent-anti-counterfeit platform can be utilized to prevent fraud in various areas, including fluorescent paints, protective coatings, flexible films, security printing, and pharmaceuticals.[25] Since **HBP1** and **HBP2** exhibit solubility, high stability, and bright fluorescence in DMSO, they can be effectively used in anticounterfeiting applications. To create anticounterfeiting security text and fingerprint, a 1 mg mL^{-1} solution of **HBP2** was coated onto filter paper in the form of
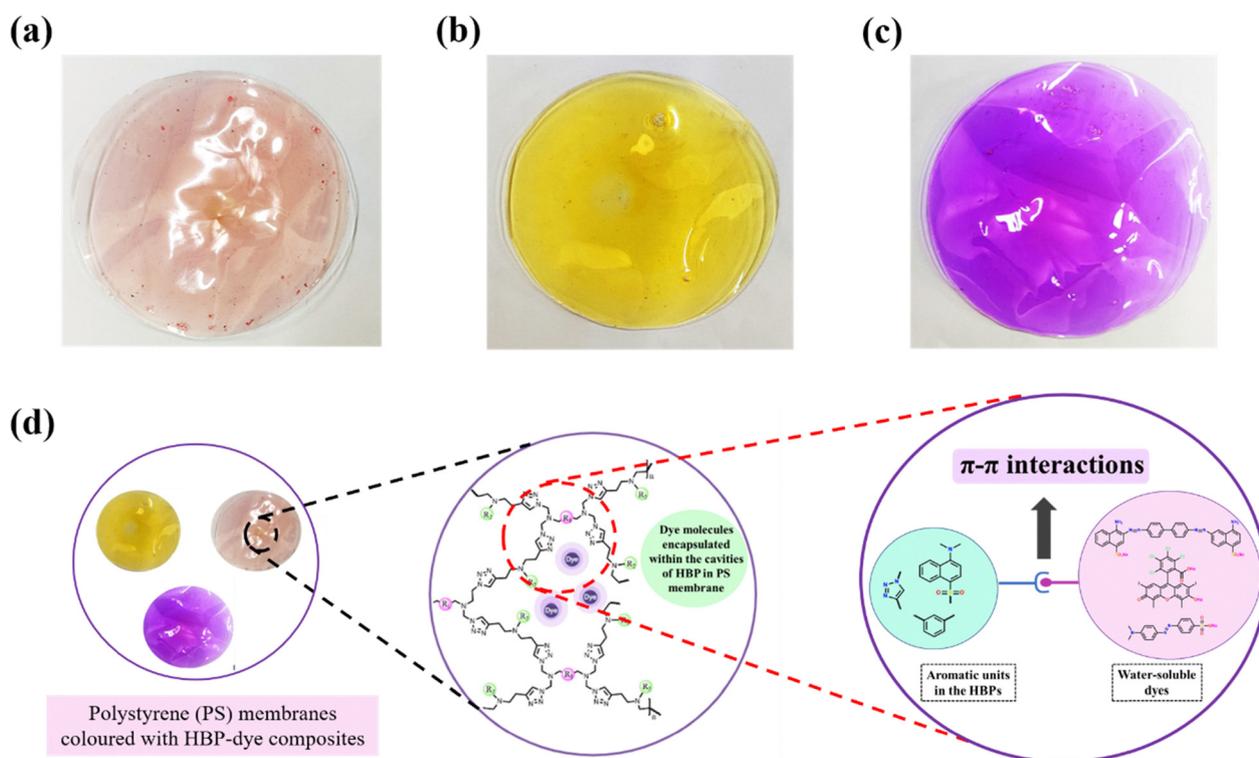
Fig. 6 Photographs of polystyrene membranes colored with (a) **HBP2**-Congo red, (b) **HBP2**-methyl orange, (c) **HBP2**-Rose Bengal composites. (d) Schematic of the interaction between the dye and HBP.

letters and a fingerprint, and then dried. These markings are invisible under normal light but become visible under UV light (Fig. 7). This invisible ink application can be used on original products to help identify counterfeit branded items, providing a reliable method for detecting forgeries.

4. Conclusion

A novel class of triazole-based hyperbranched polymers (HBPs), crafted through the copper(I)-catalyzed alkyne–azide cycloaddition (CuAAC) reaction, was synthesized. This system offered functional tunability by strategically modifying the alkyne and azide-based building blocks with diverse functionalities. The HBPs were characterized using FT-IR, ^{1}H NMR, TGA-DTA, SEM-EDAX, XRD, DSC, cyclic voltammetry, and steady-state and time-resolved spectroscopy. Through the modification of functional groups, hyperbranched polymers (HBPs) experienced changes in properties such as solubility, hydrophobicity, thermal stability, and electrochemical and photophysical characteristics. When appended with a dansyl-fluorophore, these HBPs displayed solid-state and solution-state fluorescence properties, solvatochromism, and better solubility in organic solvents. Additionally, increasing the number of aromatic moieties within the HBP structure led to a substantial enhancement in conductivity. The HBPs were employed to encapsulate four water-soluble dyes. Those incorporating the dansyl moiety, which provided solubility in organic solvents, were specifically selected for extracting dyes from the aqueous phase into the organic phase. Remarkably, the results underscored that the synergistic interplay between the hyperbranched architecture and the dansyl moiety facilitated the extraction process. Among the two HBPs with encapsulation properties, the one with more aromatic units showed higher efficiency, indicating the importance of π–π interactions between the HBPs and aromatic dyes, facilitating the process. Further investigations involved release studies to elucidate the dye-holding capacity of the HBPs. Interestingly, both **HBP1** and **HBP2** exhibited robust dye-holding capabilities, thus demonstrating minimal dye release. The remarkable ability of HBPs to firmly adhere to dyes was effectively leveraged in the coloring of plastic membranes. As anticipated, the resulting coloration of the membranes proved to be highly stable, even upon exposure to water. This underscores the pivotal role of HBPs in enhancing the longevity and reliability of coloring applications in various industries, thus improving product durability and environmental sustainability. Furthermore, the photophysical properties of fluorescent HBPs make them ideal for anti-counterfeit applications. Under UV light, **HBP2** revealed imprints of letters and fingerprints, highlighting its potential as a powerful tool for forgery prevention in various industries.

Author contributions

Mintu Porel: writing – review & editing, writing – original draft, supervision, funding acquisition, formal analysis, conceptualization.

Geethanjali Anand: writing – review & editing, writing – original draft, validation, formal analysis, data curation.

Conflicts of interest

The authors declare that they have no known competing financial interests or personal relationships that could have appeared to influence the work reported in this paper.

Data availability

The data will be made available upon request to the authors.

Supplementary information (SI) is available. See DOI: **https://doi.org/10.1039/d5ma00504c**.

Acknowledgements

Notes and references

1 B. I. Voit and A. Lederer, *Chem. Rev.*, 2009, **109**, 5924.

2 S. I. Bhat, Y. Ahmadi and S. Ahmad, *Ind. Eng. Chem. Res.*, 2018, **57**, 10754.

3 A. M. Caminade, A. Beraa, R. Laurent, B. Delavaux-Nicot and M. Hajjaji, *J. Mater. Chem. A*, 2019, **7**, 19634.

4 A. Saadati, M. Hasanzadeh and F. Seidi, *TrAC, Trends Anal. Chem.*, 2021, **142**, 116308.

5 M. Adeli and R. Haag, *J. Polym. Sci., Part A: Polym. Chem.*, 2006, **44**, 5740.

6 G. Kreutzer, C. Ternat, T. Q. Nguyen, C. J. Plummer, J. A. E. Månson, V. Castelletto and H. A. Klok, *Macromolecules*, 2006, **39**, 4507.

7 K. Uhrich, *Trends Polym. Sci.*, 1997, **12**, 388.

8 S. Mecking, R. Thomann, H. Frey and A. Sunder, *Macromolecules*, 2000, **33**(11), 3958–3960.

9 M. Arkas, L. Eleades, C. M. Paleos and D. Tsiourvas, *J. Appl. Polym. Sci.*, 2005, **97**, 2299.

10 L. Thurakkal and M. Porel, *Environ. Sci.: Water Res. Technol.*, 2023, **9**, 285.

11 S. R. Cheekatla, L. Thurakkal, A. Jose, D. Barik and M. Porel, *Molecules*, 2022, **27**, 3409.

12 E. Soršak, J. V. Valh, Š. K. Urek and A. Lobnik, *Analyst*, 2015, **140**, 976.

13 L. Albertazzi, B. Storti, L. Marchetti and F. Beltram, *J. Am. Chem. Soc.*, 2010, **132**, 18158.

14 X. Hu, L. Zhou and C. Gao, *Colloid Polym. Sci.*, 2011, **289**, 1299.

15 M. Krämer, J. F. Stumbé, H. Türk, S. Krause, A. Komp, L. Delineau and R. Haag, *Angew. Chem., Int. Ed.*, 2002, **41**, 4252.

16 N. Pérignon, A. F. Mingotaud, J. D. Marty, I. Rico-Lattes and C. Mingotaud, *Chem. Mater.*, 2004, **16**, 4856.

17 H. Kim, J. Ge, J. Kim, S. E. Choi, H. Lee, H. Lee and S. Kwon, *Nat. Photonics*, 2009, **3**, 534.

18 S. Huang and J. K. Wu, *IEEE Trans. Inf. Forensics Secur.*, 2007, **2**, 164.

19 S. Kumar, K. Achazi, C. Böttcher, K. Licha, R. Haag and S. K. Sharma, *Eur. Polym. J.*, 2015, **69**, 416.

20 E. Arunkumar, C. C. Forbes and B. D. Smith, *Eur. J. Org. Chem.*, 2005, 4051.

21 Y. Che, A. Datar, X. Yang, T. Naddo, J. Zhao and L. Zang, *J. Am. Chem. Soc.*, 2007, **129**, 6354.

22 L. R. Dalton, J. Thomson and H. S. Nalwa, *Polymer*, 1987, **28**, 543.

23 F. Schwarz, G. Kastlunger, F. Lissel, H. Riel, K. Venkatesan, H. Berke and E. Lörtscher, *Nano Lett.*, 2014, **14**, 5932.

24 A. A. Ansari, K. M. Aldajani, A. N. AlHazaa and H. A. Albrithen, *Coord. Chem. Rev.*, 2022, **462**, 214523.

25 P. Kumar, S. Singh and B. K. Gupta, *Nanoscale*, 2016, **8**, 14297.